Study on compressive stress-strain relationship of ultra-high performance concrete with coarse aggregates under and after high temperatures

Congcong Xue [1], Haoming Xu [1], Min Yu [2, *], Xiaoyong Mao [1,3], Xiaoyan Ding [1], Jianqiao Ye [4, *]

[1] School of Intelligent Manufacturing and Intelligent Transportation, Suzhou City University, Suzhou 215104, China

[2] School of Civil Engineering, Wuhan University, Wuhan, 430072, China

[3] Suzhou University of Science and Technology, Suzhou, 215009, China

[4] School of Engineering, Lancaster University, Lancaster, LA1 4YR, UK

Abstract: Uniaxial compression tests are conducted on ultra-high performance concrete (UHPC) with different volume fractions of coarse aggregates (0%, 10%, 20%, and 30%) at temperatures ranging from room temperature to 900°C, both during and after high-temperature exposure. The compressive failure modes and the stress-strain curves of the ultra-high performance concrete with coarse aggregates (CA-UHPC) under and after high temperatures are obtained. A systematic analysis of the key characteristic parameters of the stress-strain curve, including axial compressive strength, elastic modulus, and peak strain, is carried out, and respective temperature-dependent calculation formulas are proposed. Experimental results show that the failure modes under and after high temperatures are similar, both exhibiting shear failure. It is found that both the temperature and the coarse aggregate contents affect the shape of the stress-strain curve. The uniaxial compressive performance of the CA-UHPC under and after high temperatures is compared. Finally, the uniaxial compressive stress-strain relationships of the CA-UHPC under and after high temperatures are established, considering the temperature, coarse aggregate content, and steel fiber content.

Keywords: CA-UHPC; Under high temperature; After high temperature; Uniaxial compression; Stress-strain relationship

1 Introduction

UHPC is a new type of sustainable and environmentally friendly material that is increasingly used in buildings, bridges, and decoration projects. Research on the room-temperature performance of UHPC is extensive and growing [1-3]. However, UHPC is occasionally or frequently subjected to high temperature throughout its service life cycle, such as in nuclear power plant and building fire. High temperature can degrade the mechanical properties of materials, resulting in inestimable losses[4-7]. The high-temperature strength and deformation of UHPC are fundamental for calculating deformation and fire resistance of UHPC structures under high temperature or fire. These properties are also essential for predicting the residual mechanical properties and post-fire structural damage of UHPC structures.

Generally, UHPC is classified into ultra-high performance concrete with coarse aggregates (CA-UHPC) and reactive powder concrete without coarse aggregate (RPC) [8]. Numerous researches have reported on the high-temperature strength of UHPC [6, 9-14], while research on the stress-strain relationship of UHPC after high temperature has mainly focused on RPC[15-19]. For example, Tai[16] and Zheng et al. [17, 18] conducted uniaxial compression tests on fiber reinforced RPC after high temperature, analyzing the effects of high temperature and fiber contents on the stress-strain curve and characteristic parameters. They found that at 600°C, UHPC exhibited the highest strain. Zheng et al. [17, 18] indicated that, compared to ordinary concrete and high-strength concrete, hybrid fiber-reinforced RPC has superior high-temperature resistance and provided an equation for the stress-strain curve of RPC after high temperature. Fan[19] carried out axial compression tests on aluminate cement-based UHPC prisms after high temperature, presenting stress-strain curves and characteristic parameters. Formulas for

calculating these parameters and a uniaxial compressive constitutive model of UHPC to simulate fire effects were proposed. All the above studies offer valuable tools for predicting the bearing capacity and aiding the structural repair of RPC structures after high temperature.

Research on the stress-strain relationship of UHPC under high temperature primarily focus on RPC. Xu[20] and Zheng et al. [21, 22] conducted uniaxial compression tests on fiber reinforced RPC at temperatures ranging from room temperature to 800℃. The results indicate that different steel fiber contents (1%~3%) do not significantly affect the characteristic parameters of the stress-strain curve of RPC under high temperature, such as peak strain, initial elastic modulus, and peak secant elastic modulus. They also proposed a compressive constitutive model for RPC under high temperature. Huang et al. [23] studied uniaxial compression of CA-UHPC with a certain amount of coarse aggregates under high temperature, and presented the stress-strain curves and characteristic parameters. The proposed stress-strain relationship equation was validated by the experimental data.

In summary, although there have been some studies on the uniaxial compressive stress-strain relationship of RPC under and after high temperatures, research on CA-UHPC, particularly on UHPC with varying coarse aggregate contents, remains limited. The distinctive properties of coarse aggregates and cementitious matrix suggest that the inclusion or exclusion of coarse aggregates in UHPC significantly impacts its high-temperature mechanical properties, warranting further investigation. In view of this, this paper studies the uniaxial compressive mechanical properties of CA-UHPC with four different coarse aggregate contents under and after high temperatures, ranging from room temperature to 900°C. The focus is on analyzing the influence of mix ratio, temperature range, and temperature state on uniaxial compression performance, in an attempt to provide fundamental experimental data and theoretical support for fire resistance prediction, design of engineering structures under high temperature, and post-fire evaluation and repair of engineering structures.

2 Experimental program

2.1 Raw materials and mix proportion

Based on previous work[9, 24, 25], the influence of steel fibers on thermal and mechanical properties of UHPC is not significant. Therefore, the volume fraction of steel fibers in the mix proportion is set as a constant (2%), and only the variation of coarse aggregates is considered in the mix proportion. The volume fractions of coarse aggregates in the UHPC are 0, 10%, 20% and 30%, respectively, representing a total of four different CA-UHPC mixes. The specimens are designated as CA0, CA10, CA20, and CA30, respectively, where CA0 represents the sample with a volume fraction of 0 coarse aggregates.

Table 1 Mix proportion of the CA-UHPC (unit: kg/m^3) [9, 24]

Mixture ID	Cement	Silica fume	Fly ash	Water	Water reducer	Quartz sand	Steel fibers	Coarse aggregates
CA0	703.6	131.9	44.0	140.7	26.4	1205.0	158.3	0.0
CA10	630.1	118.1	39.4	126.0	23.6	1079.0	141.8	252.0
CA20	557.2	104.5	34.8	111.4	20.9	954.2	125.4	501.5
CA30	485.6	91.1	30.4	97.1	18.2	831.7	109.3	746.7

2.2 Heating regime

According to the Eurocode 2 [26] and Guo [27], the compressive strength of concrete is only 5% to 15% of that at room temperature when the temperature reaches 900℃. Therefore, the temperatures for tests under and after high temperatures are designed to be room temperature, 100°C, 300°C, 500°C, 700°C and 900°C, for a total of 6 temperature levels. The main purpose of this study is to investigate the mechanical properties of CA-UHPC under and after constant high temperature. Therefore, only the final temperature of the samples is concerned, and the heating process of the samples is ignored. To reduce spalling of the CA-UHPC during heating, a hating rate of 1 ℃/min is used from 200℃ to 400℃, and 5 ℃/min for all other temperature range. The temperature is maintained constant for 3 h and 1 h before and after 500°C, respectively, to ensure uniform temperature distribution within the specimens and to save time.

2.3 Compression test

The uniaxial compression test uses prisms of 100 mm × 100 mm × 300 mm. Fore mix proportions, six temperature levels, and three repeated tests are conducted on a total 144 specimens. The specific design is shown in Table 2.

Table 2 Design of uniaxial compression specimens

Type of test	Size/mm	Number of mix proportion	Number of temperature level	Repetition	Number of specimen
After high temperature	100×100×300	4	6	3	72
Under high temperature	100×100×300	4	6	3	72

Since the compression specimens under high temperatures are tested inside the high-temperature furnace, Direct deformation measurement is not convenient. Considering that the stiffness of an ordinary test machine may not be sufficient to ensure accurate measurement of the descending branch of the CA-UHPC stress-strain curve, a rigid high-temperature resistant frame is designed and manufactured. This frame allows the deformation of the upper and lower ends of the specimen to be measured outside the electric furnace (Fig. 1(b)). The rigid high-temperature resistant frame includes two parts: an external rigid loading frame and internal measuring component. The rigid loading frame consists of upper beams, columns, and lower beams that are connected to provide variable stiffness as required, as shown in Fig. 1(a). The measuring component consists of the round plates, vertical plates and extension bars, as shown in Fig. 1(b)-internal. The design has been patented in China [28]. The uniaxial compression test after high temperature is conducted using a 250 t MTS universal testing machine. The deformation of the CA-UHPC is measured using strain displacement sensors.

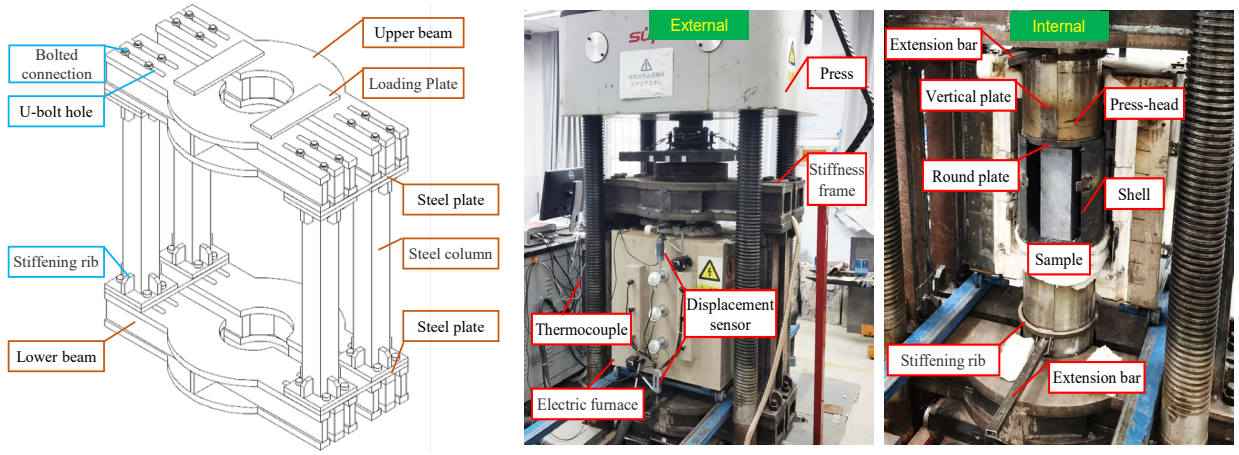

(a) Schematic diagram of the loading frame (b) Test set-up

Fig. 1 High-temperature uniaxial compression test

3 Tests at different temperatures

3.1 Under high-temperature tests

3.1.1 Failure mode

The failure morphology of the prisms subjected to uniaxial compression under high temperature is shown in Fig. 2, revealing visible damage patterns. All CA-UHPC specimens exhibit diagonal cracks with penetrating cracks forming the main cracks. The angle between the main crack and the vertical direction increases slowly with the increase of temperature, resulting in the overall failure angle ranges from 62° to 84°. The specimens are subjected to shear failure.

As the temperature increases, the number of diagonal cracks increases, and plastic failure of the prisms become more apparent. When the temperature is below 700℃, the shear failure angles do not obviously change. When the temperature reaches 900℃, the inclined fracture zone is wider and primarily occurs in the middle of the specimen. Despite some fragments falling off, the specimens remain relatively well-integrated. As the content of coarse aggregates increases, the inclination angle of the main crack increases, however, coarse aggregate contents generally have little influence on the failure mode of the specimen.

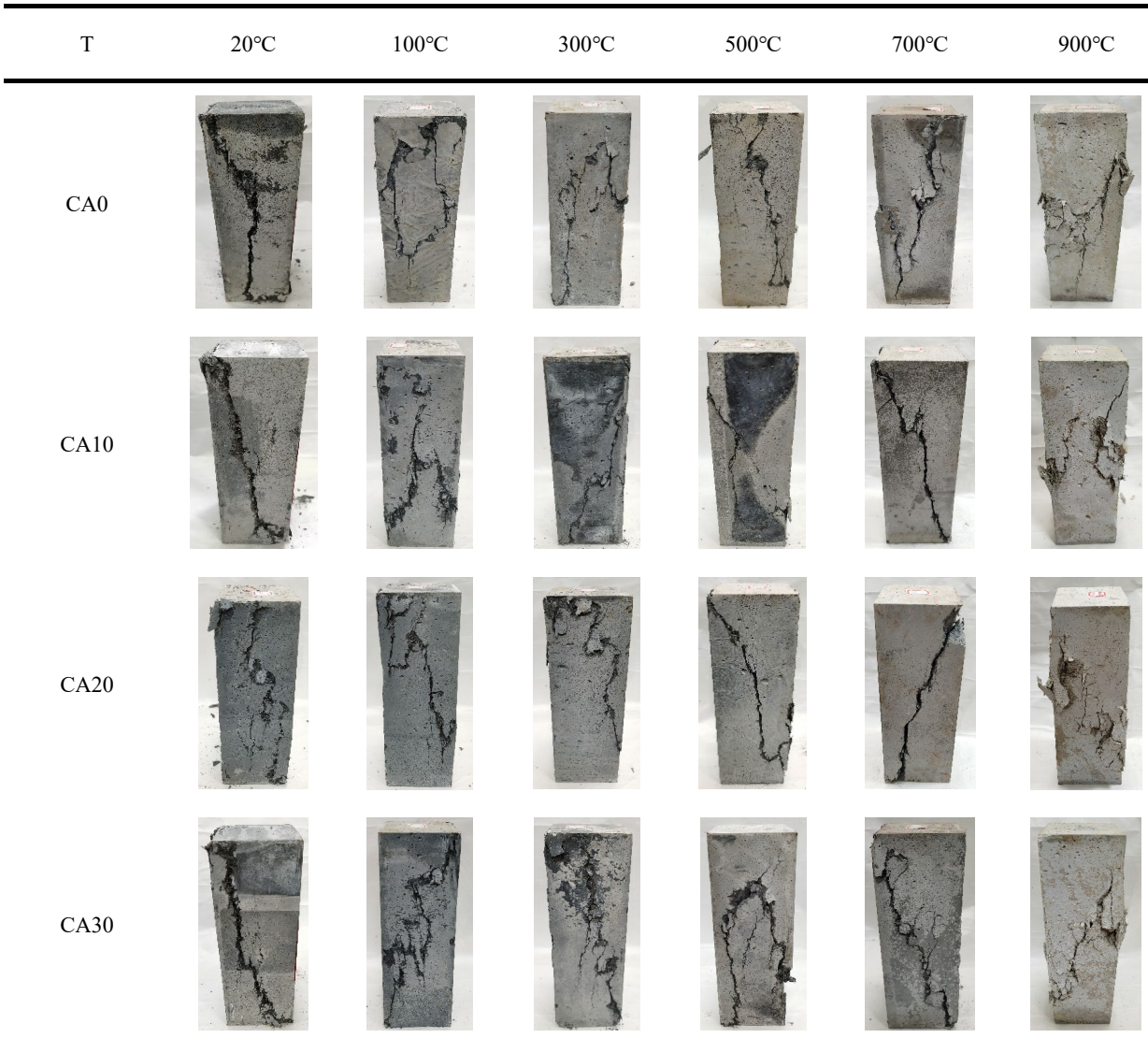

Fig. 2 Compressive failure characteristics of specimens under high temperature

3.1.2 Stress-strain curve

The complete stress-strain curves of the CA-UHPC under high temperature are plotted in Fig. 3. From Fig.

3, it can be seen that for a fixed mix ratio, the stress-strain curves show that with an increase of temperature, the elastic modulus and the peak stress of the CA-UHPC decrease, while the peak strain increases. The peak strain of the CA-UHPC at room temperature range from 2350με to 3150με. According to the Code for Design of Concrete Structures (GB 50010-2010) [29], the peak strain of ordinary concrete is approximately 2200με, and the peak strain of high-strength concrete is about 2500με to2600με. The peak strain of the current CA-UHPC is obviously higher than that of ordinary concrete and can exceed that of high-strength concrete.

In addition, the coarse aggregate contents also affect the shape of the stress-strain curve of the CA-UHPC. Under the same temperature, CA-UHPC with higher coarse aggregate contents exhibits higher peak stress and peak strain. The results also show that adding more coarse aggregates increases the slope of the ascending branch of the stress-strain curves, thereby enhancing the initial stiffness of the CA-UHPC.

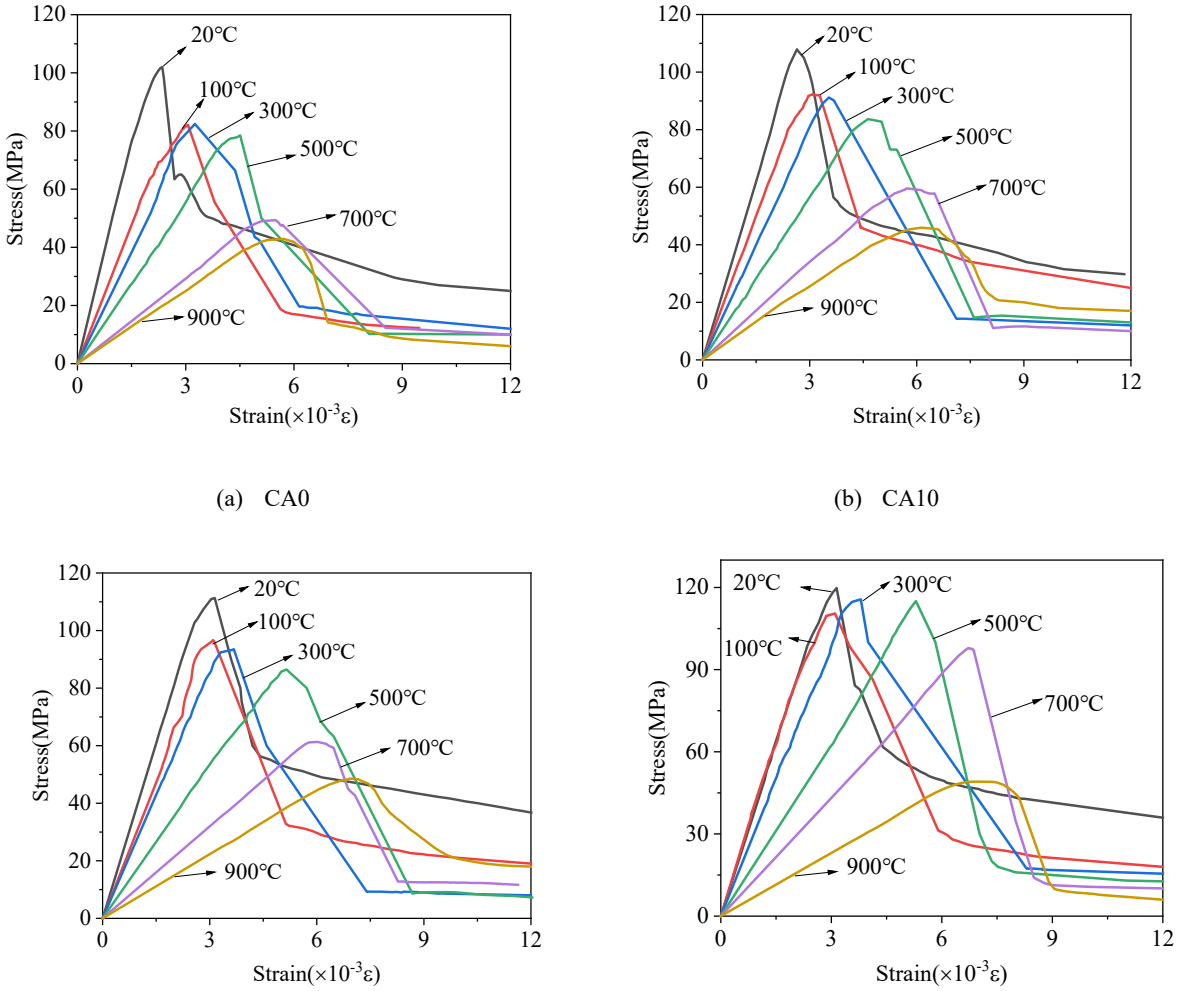

Fig. 3 The complete stress-strain curves of the CA-UHPC under high temperature

In order to study the effect of temperature on the stress-strain curve of CA-UHPC more effectively, the stresses and strains in Fig. 3 are normalized by their respective peak stresses and peak strains at room temperature. The normalized stress-strain curves are shown in Fig. 4. Overall, the effect of the temperature on the ascending segment of the normalized stress-strain curve is not significant, which is consistent with the patterns observed in ordinary concrete [27, 30, 31]. However, a significant difference is observed in the descending segment of the normalized stress-strain curve when the stress ratio is below 0.6. Generally, a higher temperature results in a steeper descending segment, leading to a smaller area under the descending segment of the curve. This is partially

attributable to the softening of the steel fibres inside the CA-UHPC under high temperature, especially at 500℃ or above, causing more cracks and thus a steeper descending segment of the stress-strain curves.

By comparing the normalized stress-strain curves of the CA-UHPC with different coarse aggregate contents under the same temperature, it is evident that with the increase of coarse aggregate contents, the ascending branch of the stress-strain curve has a longer linear segment, indicating a longer-lasting linear elasticity.

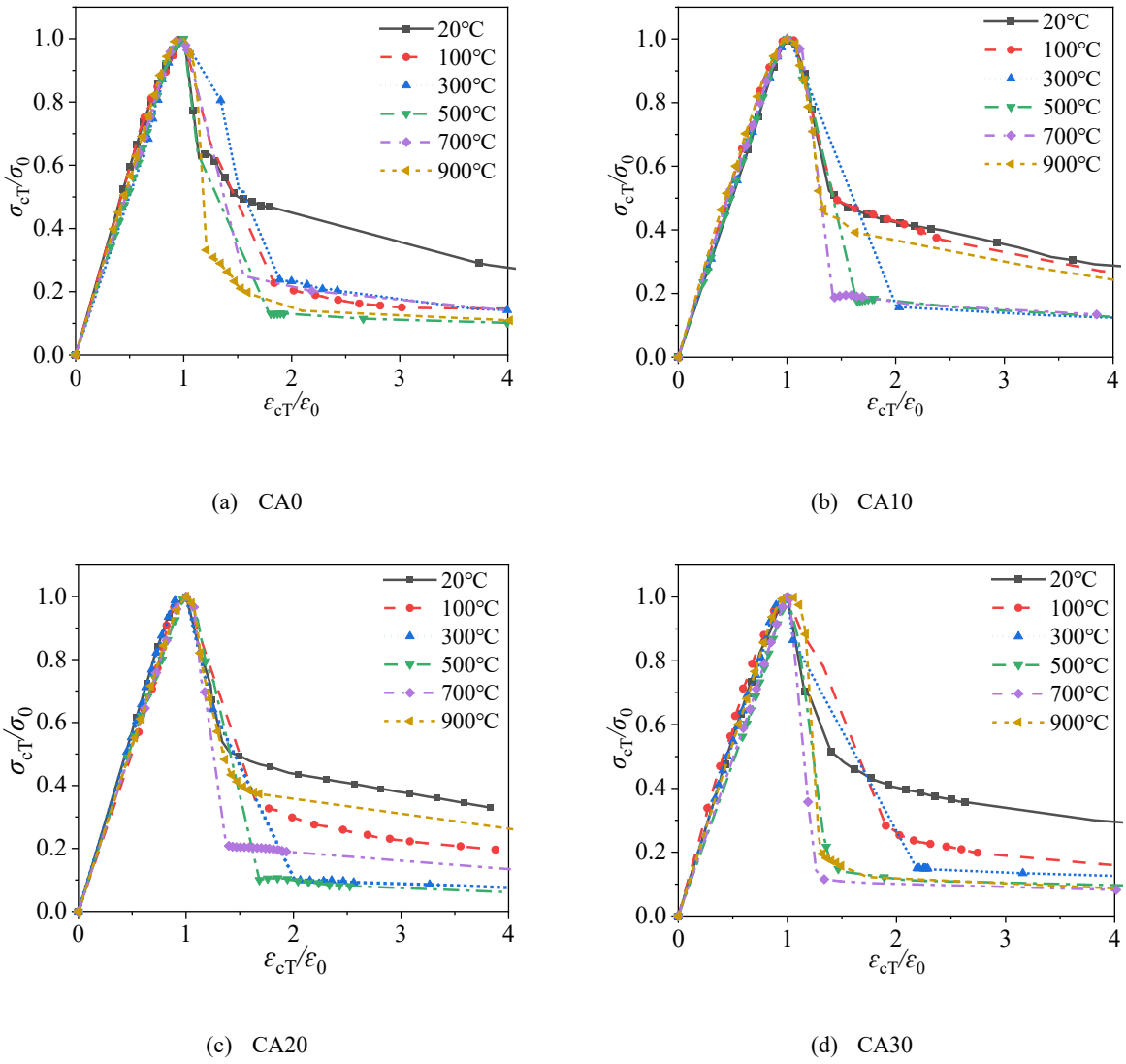

(a) CA0 (b) CA10

(c) CA20 (d) CA30

Fig. 4 Normalized stress-strain curves of the CA-UHPC under different high temperatures

3.2 Post high temperature tests

3.2.1 Failure mode

The failure morphology of the prisms subjected to uniaxial compression after high temperature is shown in Fig. 5.The prisms exhibit a distinct main crack along the diagonal direction, indicating shear failure. The angle between the main crack and the vertical direction increases with rising temperature, ranging from 61° to 83°. When the temperature reaches 900℃, the prisms break into two pieces after compression, losing their integrity. Overall, coarse aggregate contents have little effect on the failure mode of the prisms.

Comparing the failure morphology of the specimens under and after high temperatures, it is observed that after experiencing the same maximum temperature, the specimens under high temperature shows more branch-like cracks on the surface, exhibiting more plastic characteristics.

T	100℃	300℃	500℃	700℃	900℃
CA0					
CA10					
CA20					
CA30					

Fig. 5 Compressive failure characteristics of specimens after high temperature

3.2.2 Stress-strain curve

The stress-strain curves of the CA-UHPC after high temperature are plotted in Fig.6.

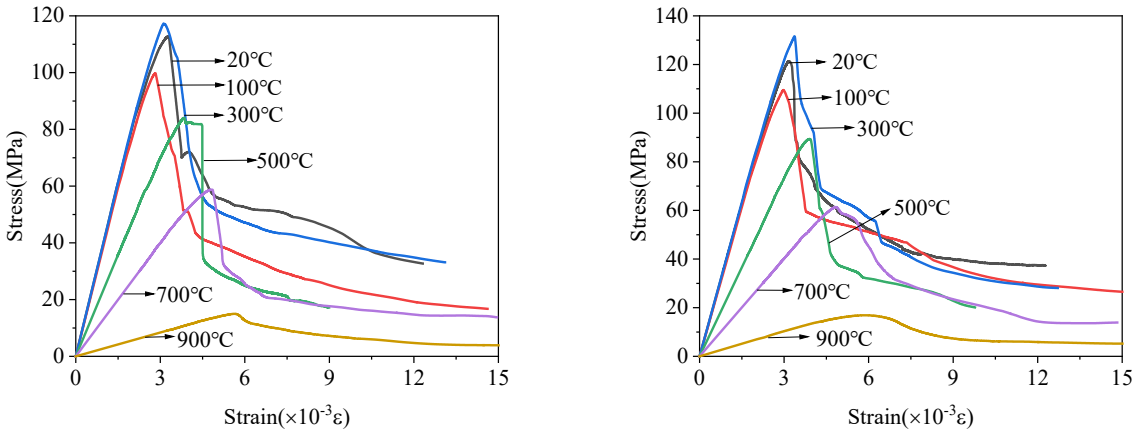

(a) CA0 (b) CA10

Fig. 6 The complete stress-strain curves of the CA-UHPC after high temperature

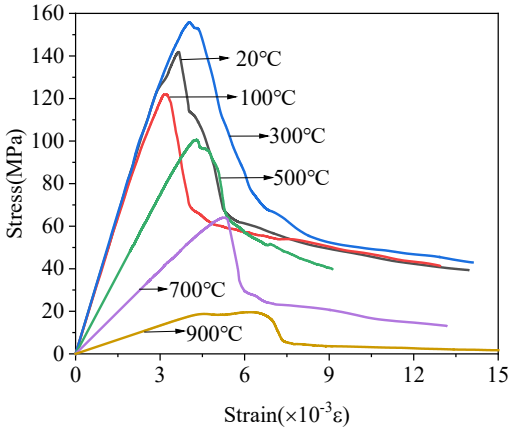

(c) CA20

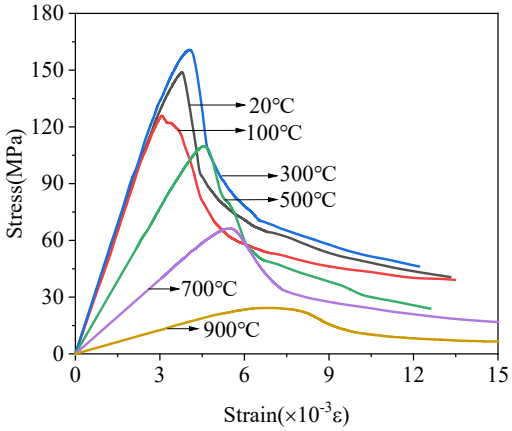

(d) CA30

Fig. 6 (Continue)

In general, the stress-strain curves of the CA-UHPC with a fixed mix ratio show a decreasing trend in elastic modulus and peak stress, and an increasing trend in peak strain with increasing temperature in Fig. 6. Specifically, the peak stress of the curves reaches its maximum at 300°C, and steadily decreases with further temperature increases. The elastic modulus increases slightly at 300°C, and then decreases continuously with increasing temperature. The amounts of coarse aggregates also influence the shape of the stress-strain curves after high temperature, with a similar effect observed under high temperature conditions.

The normalized stress-strain curves after high temperature are shown in Fig. 7. As the temperature increases, the area under the ascending segment of the curve increases slightly. The descending segment of the curves becomes steeper with rising temperature, and this trend of faster declining after the peak is more pronounced after 500°C.

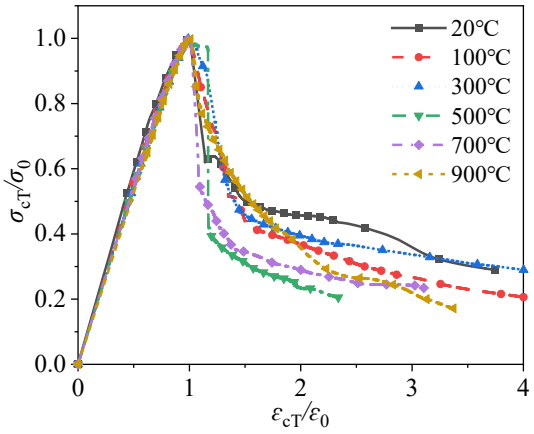

(a) CA0

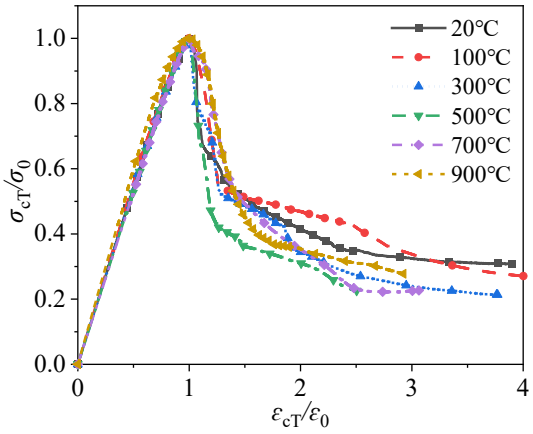

(b) CA10

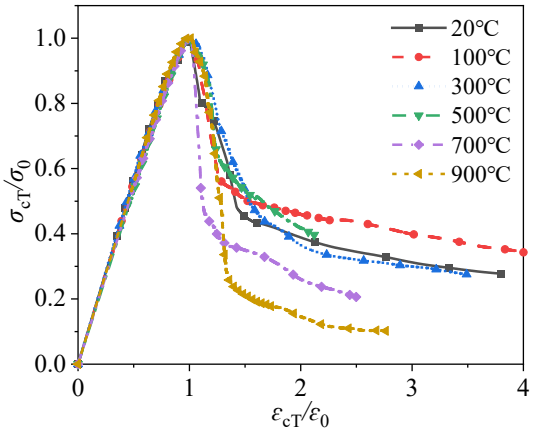

(c) CA20

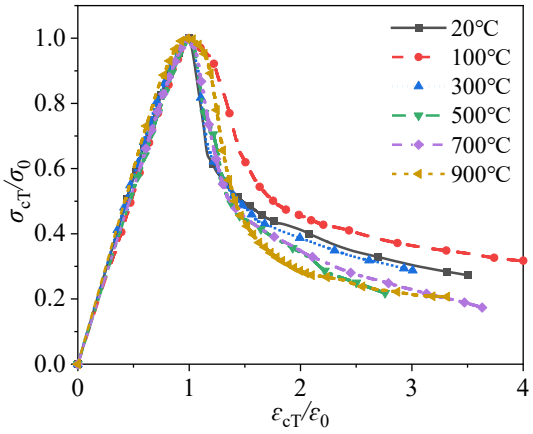

(d) CA30

Fig. 7 Normalized stress-strain curves of CA-UHPC after different high temperatures

Comparing the influence of coarse aggregate contents on the normalized stress-strain curve, it can be seen that as the coarse aggregate contents increase, the ascending segment of the curves varies insignificantly, while the descending segment varies significantly. Therefore, the influence of coarse aggregate contents on the descending segment should be taken into account when formulating the stress-strain relationship of the CA-UHPC.

4 Characteristic parameters of the stress-strain curve

4.1 Axial compressive strength

For each mixture ratio, three CA-UHPC samples are grouped and tested for the compressive strength. Fig. 8 shows the averaged compressive strength of each group under different temperatures.

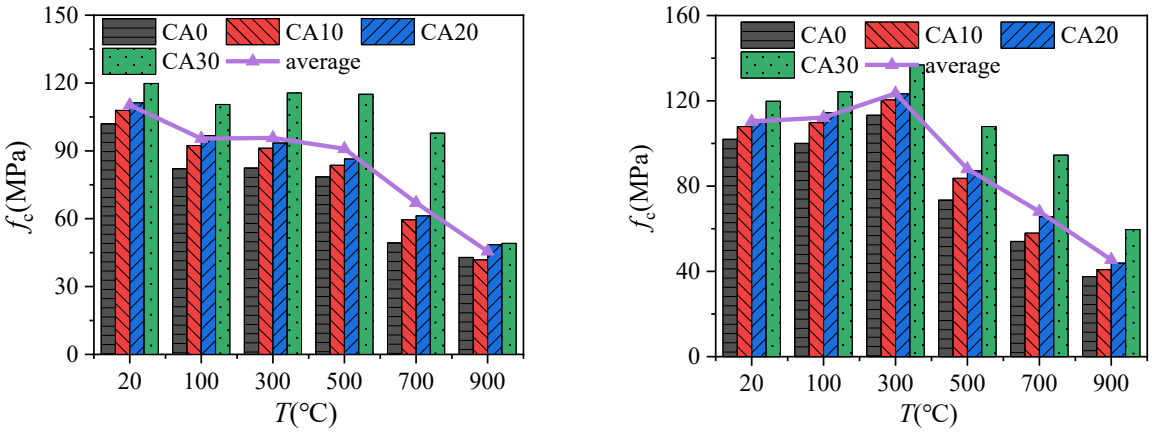

(a) Under high temperature (b) After high temperature

Fig. 8 Axial compressive strength of the CA-UHPC under and after high temperatures [9]

4.1.1 Analysis of the influencing factors

Fig. 8(a) shows that the compressive strength of the CA-UHPC under high temperature decreases with the increase of temperature. At 500℃, the compressive strength is reduced by 5 MPa to 25 MPa, representing a 4% to 23% reduction. When the temperature reaches 700℃ to 900℃, the compressive strength decreases significantly. At 900℃, the compressive strength is about 59 MPa to 71 MPa lower than that at room temperature, a decrease of 56% to 61%. Fig. 8(b) shows that the compressive strength of the CA-UHPC after heating increases up to 300℃. Beyond 300℃, the compressive strength exceeds the room temperature value by 11 MPa to 17 MPa, or 11% to 14%. This is because as the temperature gradually rises to 300℃, loss of free water and rehydration occurs, as well as the median diameter of pores is the smallest, which corresponds to an increase in compressive strength[9]. After 300ºC, the compressive strength decreases as the temperature increases. At 900℃, the compressive strength is reduced by 60 MPa to 67 MPa, representing a decrease of 50% to 63%.

In summary, the compressive strength of the specimen after heating to a temperature is greater than that under the same temperature, which can be explained by the fact that the mass loss of the samples after high temperature is smaller than that under high temperature[9]. Compressive strength increases with higher coarse aggregate contents. Under compression, microcracks typically bypasses coarse aggregates, forming a longer failure path. Observations from the tests indicate that thermal degradation of coarse aggregates is less severe than that of the CA-UHPC matrix, and the reinforcement effect of coarse aggregates on CA-UHPC is more prominent. Therefore, CA-UHPC with more coarse aggregates exhibits greater compressive strength.

4.1.2 Predictive model

Based on the change patterns of compressive strength of the prisms under and after high temperature, the predictive models for the reduction coefficient of the compressive strength are established, respectively. The

reduction coefficient (k) is defined as the ratio of the compressive strength at temperature T (f_{cT}) to the compressive strength of the same concrete at room temperature (f_{c0}). The specific fitting process can be referred to reference [9].

The reduction coefficient of the prismatic compressive strength under high temperature is,

$$k_U = \frac{f_{cT}}{f_{c0}} = -6.67\times10^{-4}T + 1.01, \quad 20°\text{C} \le T \le 900°\text{C} \tag{1}$$

The average value and coefficient of variation of the ratio of the predictions of Eq.(1) to experimental results are 0.97 and 0.122, respectively.

The reduction coefficient of the prismatic compressive strength after high temperatures is,

$$k_F = \begin{cases} 1, & 20°\text{C} \le T \le 300°\text{C} \\ -9.84\times10^{-4}T + 1.3, & 300°\text{C} < T \le 900°\text{C} \end{cases} \tag{2}$$

The average value and coefficient of variation of the ratio of the predictions of Eq.(2) to experimental results are 0.99 and 0.0998, respectively.

4.2 Elastic modulus

Elastic modulus is a key indicator for measuring the deformation ability of materials, and also a crucial parameter for analyzing the mechanical properties of materials. In this study, the elastic modulus of the CA-UHPC is taken as the secant modulus at 70% of the peak stress in the ascending segment of the stress-strain curve.

4.2.1 Analysis of the influencing factors

The elastic modulus of the CA-UHPC at different temperatures is plotted in Fig. 9, where E_{c0} and E_{cT} represent the elastic modulus at room temperature and temperature *T*, respectively. From Fig. 9(a) and (b), the elastic modulus of the specimen under high temperature decreases almost linearly as the temperature increases. Specifically, except for a slight increase in the elastic modulus of CA30 at 100℃, the elastic moduli of other CA-UHPC specimens decrease significantly, by about 20%. From 300℃ to 700℃, the elastic modulus decreases at a relatively consistent rate. At 700 ℃, the elastic modulus decreases to about 30% of that at room temperature. When the temperature reaches 900℃, the elastic modulus decreases slowly to between 7.5 GPa and 8.5 GPa, which is less than 20% of the elastic modulus at room-temperature. The peak stress at 900℃ decreases to 40% of the peak stress at room temperature (Fig. 3). Obviously, the reduction of elastic modulus caused by high temperature is greater than that of peak stress, indicating that high temperature has a greater influence on the deformation of the CA-UHPC. This is also the significance of studying high-temperature deformation of CA-UHPC. From Fig. 9(c) and (d), the elastic modulus of the CA-UHPC after high temperature initially increase and then decreases, which is similar to the trend of peak stress in the CA-UHPC after high temperature (Fig. 8). Specifically, the elastic modulus reaches its maximum value at 300℃, with an increase of about 2.4%; Subsequently, as the temperature increases, the elastic modulus decreases almost linearly. The reason for the increase in elastic modulus and compressive strength at 300℃ is consistent. After 900℃, the elastic modulus decreases to below 5 GPa, which is less than 10% of that at room temperature.

By comparing the influence of the coarse aggregate content (Fig. 9(b) and (d)), it can be seen that the elastic modulus under high temperature increases with the increase of the coarse aggregate content. The elastic modulus of CA30 is significantly higher than that of other CA-UHPC. Whereas the elastic modulus after high temperature is not significantly affected by the coarse aggregate content.

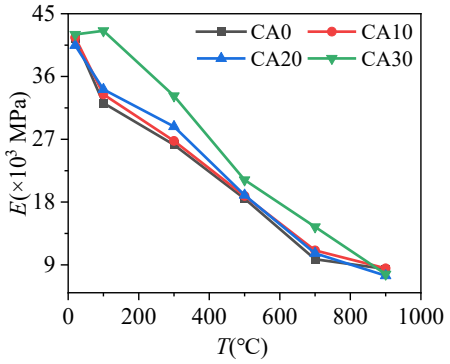

(a) Elastic modulus under high temperature

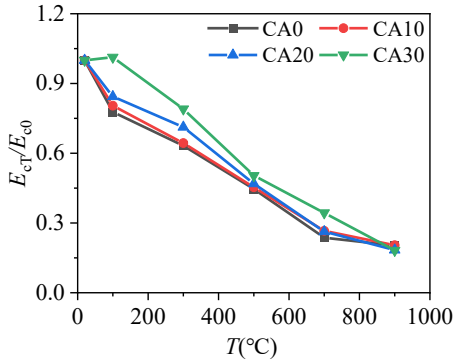

(b) Normalized elastic modulus under high temperature

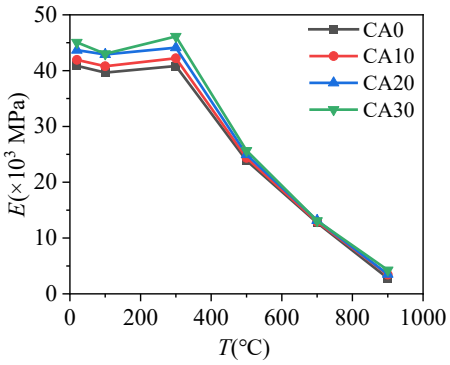

(c) Elastic modulus after high temperature

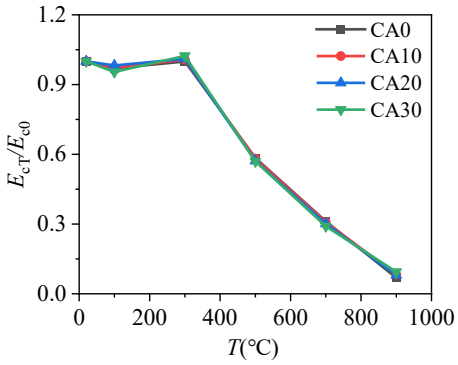

(d) Normalized elastic modulus after high temperature

Fig. 9 Elastic modulus versus temperature

4.2.2 Predictive model

To better predict the elastic modulus of the CA-UHPC under high temperature, a literature review was conducted on the elastic modulus of different types of concrete such as ordinary concrete [29,32], ultra-high strength concrete [33], RPC [34], and UHPC [35] under high temperature, which are plotted in Fig. 10 along with the experimental results of the current CA-UHPC. As can be seen from Fig. 10, the elastic modulus can be divided into two categories. The first one includes the elastic modulus of ordinary concrete (Guo [32]) and ultra-high strength concrete (Xiong [33]), which decrease linearly with increasing temperature. The second category is the elastic modulus of ordinary concrete (Eurocode 4 [36]), RPC (Luo [34]) and UHPC (Kodur [35]), which decrease nonlinearly. The elastic modulus of the current CA-UHPC under high temperature decreases slowly with the increase of temperature, which is close to Xiong's model. Based on the experimental results, the following expression for the elastic modulus of the CA-UHPC under high temperature is obtained through regression,

$$\frac{E_{cT}}{E_{c0}} = -\left(\frac{T-20}{1000}\right)+1, \quad 20℃ \le T \le 900℃ \tag{3}$$

The average value and coefficient of variation of the ratio of the predictions of Eq.(3) to experimental results are 1.01 and 0.203, respectively.

Similarly, based on literature research, the elastic modulus of different types of concrete (NSC[37, 38]、RPC[17] and UHPC[15]) after high temperature is compared with the experimental values of the CA-UHPC, as shown in Fig. 11. It is evident that the predictive formulas from the literature are rather complex. Considering the convenience and safety of the model used in practical engineering, the increase of elastic modulus at 300℃ is ignored, and a linear prediction model of the normalized elastic modulus of the CA-UHPC after high temperature is established,

$$\frac{E_{cT}}{E_{c0}} = -0.92\left(\frac{T-20}{1000}\right)+1, \quad 20℃ \le T \le 900℃ \tag{4}$$

The average value and coefficient of variation of the ratio of the predictions of Eq.(4) to experimental results are 1.05 and 0.183, respectively.

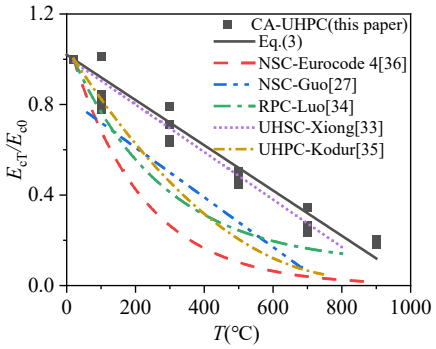

Fig. 10 Comparison of normalized elastic modulus of different kinds of concrete under high temperature

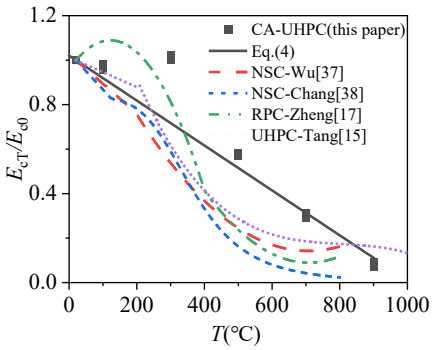

Fig. 11 Comparison of normalized elastic modulus of different kinds of concrete after high temperature

4.3 Peak strain

Peak strain is the strain corresponding to the peak stress, which reflects the deformation ability of the material affected by high temperature. The following discussion examines the effects of temperature and coarse aggregates on the high-temperature peak strain.

4.3.1 Analysis of the influencing factors

The peak strains of the CA-UHPC under and after high temperatures are plotted in Fig. 12(a) and (c), respectively, and their respective normalized peak strain are plotted in Fig. 12(b) and (d), where ε_{c0} and ε_{cT} are the peak strain at room temperature and temperature T, respectively. From Fig. 12(a) and (b), it can be seen that the peak strain of the CA-UHPC increases continuously with the rising temperature. Generally, the peak strain under high temperature increases slowly at temperatures below 300°C and above 700°C, and increases rapidly between 300°C and 700°C. Specifically, the peak strain at 300°C is 1.2 to 1.4 times of that at room temperature. While at 700°C, it is more than twice of that at room temperature. At 900°C, the peak strain reaches the maximum, up to 2.4 times of that at room temperature. In terms of the increasing rate, the peak strain of all the CA-UHPC has the largest increase at 500°C relative to 300°C, ranging from 31% to 40%, with the peak strain of CA20 increased by 40%. In contrast, the peak strain of CA20 at 100°C shows a slight decrease of 1% relative to room temperature.

Fig. 12(c) and (d) show that the peak strain of the CA-UHPC after high temperature decreases first and then increases with the rising temperature, forming a typical convex shape, which contrasts significantly with the trend under high temperature. Specifically, below 300°C, the peak strain increases slowly or even decreases slightly as the temperature increases. The peak strain increases much faster when the temperature is above 300°C. This is in line with the increase in peak stress and elastic modulus after high temperature (see Fig. 8 and Fig. 9). The peak strain after exposure to 300°C is 1 to 1.11 times of that at room temperature, and the peak strain after exposure to 900°C is 1.8 to 1.9 times of that at room temperature. The peak strain after experiencing 100°C shows the smallest increase relative to the room temperature, at -13%; while the peak strain after experiencing 700°C shows the largest increase relative to 500°C, at up to 26%. As observed also in [9], it can be concluded that exposure to excessively high temperature leads to decomposition of hydrates in the CA-UHPC, resulting in cracks and pores, reducing the effective cross-sectional area of compression, and ultimately causing a continuous increase in peak strain at high temperature.

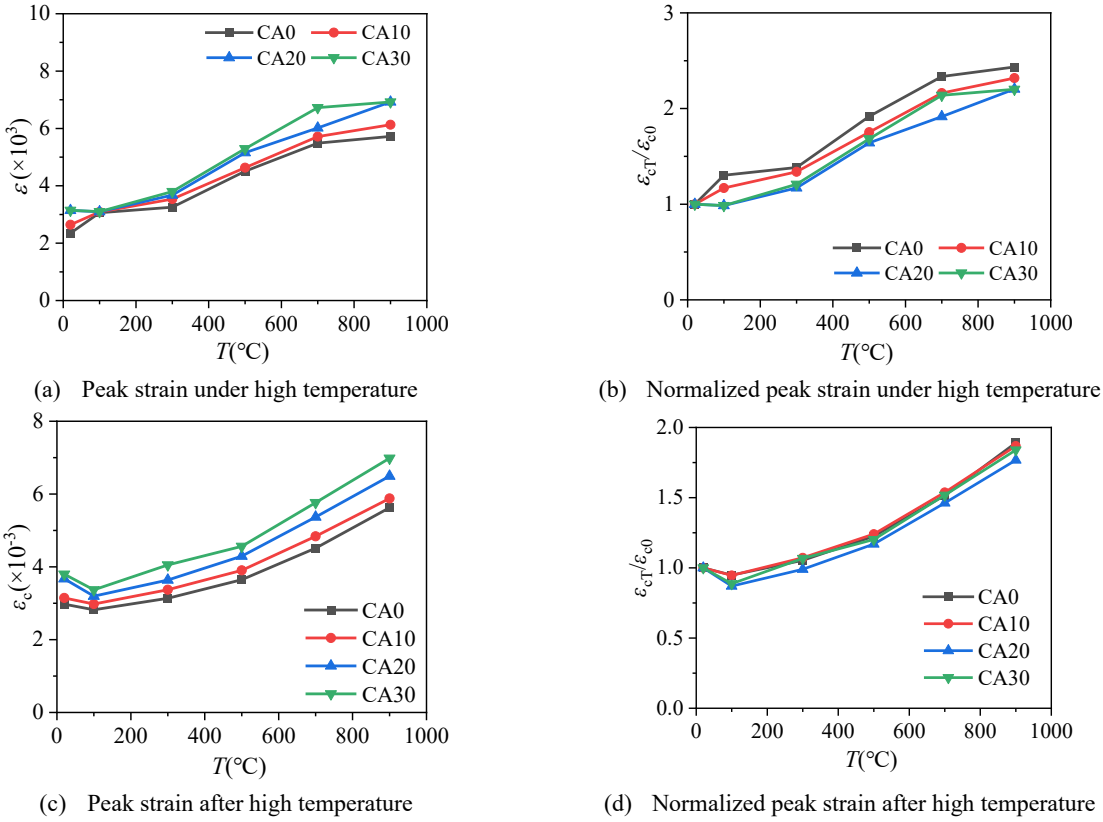

(a) Peak strain under high temperature

(b) Normalized peak strain under high temperature

(c) Peak strain after high temperature

(d) Normalized peak strain after high temperature

Fig. 12 Peak strain versus temperature

The influence of different coarse aggregate contents on the high-temperature peak strain follows a relatively consistent pattern (Fig. 12(a) and (c)). With the increase of coarse aggregate contents, the peak strain both under and after exposure to high temperatures increases approximately linearly (Fig. 12(b) and (d)). From the above analysis of the stress-strain curves of the CA-UHPC under and after high temperatures, it can be concluded that the addition of coarse aggregates can increase the axial compressive strength and the peak strain. The is because the coarse aggregates have relatively high strength, and the degradation of coarse aggregates caused by high temperature is less severe than that of the matrix. However, the difference in the thermal expansion coefficients of the coarse aggregates and the matrix at high temperature can also cause inconsistent deformation within the CA-UHPC, thereby generating of thermal cracks.

4.3.2 Predictive model

Based on the test results for peak strain under high temperature, the normalized peak strain of the CA-UHPC can be analytically presented by the following linear predictive model with respect to temperature T,

$$\frac{\varepsilon_{cT}}{\varepsilon_{c0}} = 1.51\left(\frac{T-20}{1000}\right)+1, \quad 20℃ \le T \le 900℃ \tag{5}$$

The average value and coefficient of variation of the ratio of the predictions of Eq.(5) to experimental results are 1.02 and 0.088, respectively.

For comparison, the peak strains of ordinary concrete, RPC, and UHPC under high temperature, which are predicted by EC2 (NSC) [26], Guo (NSC) [32], Luo (RPC) [34], and Kodur (UHPC) [35], respectively, are plotted in Fig. 13 along with the experimental results and the predictions of the current paper. In general, the normalized peak strain of all concrete types under high temperature increases continuously with the increase of temperature. Based on the curve characteristics of the above predictive models, they can be divided into two categories. The first category is the predictive models of EC2, Luo, and Kodur, which show an accelerated increase in peak strain with increasing temperature. The difference is that EC2 predicts that the peak strain of NSC remains unchanged above 600℃, whereas the peak strain of RPC and UHPC continue increasing up to 750℃. The second category is the predictive models of Guo and this paper, showing a linear and gradual increase of the

peak strain with rising temperature. It can be concluded that peak strain of the CA-UHPC under high temperature increases more slowly than that of NSC and RPC as temperature increases, which is consistent with the previous conclusion that the peak stress and elastic modulus of the CA-UHPC under high temperature decrease slowly with increasing temperature.

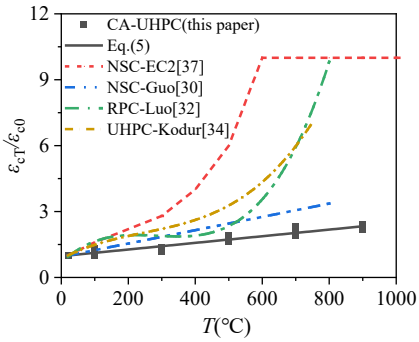

Fig. 13 Comparison of normalized peak strain of different kinds of concrete under high temperature

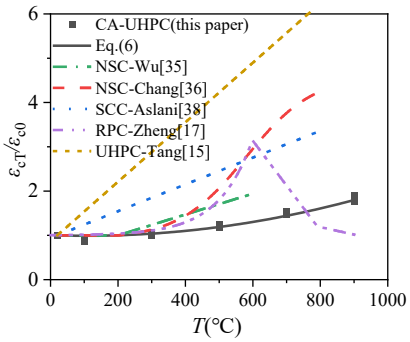

Fig. 14 Comparison of normalized peak strain of different kinds of concrete after high temperature

Similarly, based on the characteristics of the peak strain of the CA-UHPC after high temperature, the following predictive model is proposed.

$$\frac{\varepsilon_{cT}}{\varepsilon_{c0}}=1-0.22\left(\frac{T-20}{1000}\right)+1.28\left(\frac{T-20}{1000}\right)^2,\quad 20°C\le T\le 900°C \tag{6}$$

The average value and coefficient of variation of the ratio of the predictions of Eq.(6) to experimental results are 1.01 and 0.044, respectively.

The normalized peak strain of the current CA-UHPC after high temperature is compared with that of NSC[35,36]、SCC[39]、RPC[17] and UHPC without coarse aggregates [15] in Fig. 14. In general, the normalized peak strain of the concrete, except RPC, increases continuously with increasing temperature. From the room temperature to 300℃, the normalized peak strain of the CA-UHPC is close to that of NSC and RPC. After exceeding 300℃, the normalized peak strain of the CA-UHPC becomes significantly smaller than that of other concrete. It can be concluded that the rate of increase in peak strain of the CA-UHPC after high temperature is slower than that of NSC and RPC, and after 300℃, the increase in peak strain of the CA-UHPC after high temperature is similar to that under high temperature.

5 Stress-strain equation

5.1 Stress-strain equation under high temperature

(1) Room temperature parameters of the equation

The stress-strain curve of the CA-UHPC at room temperature is divided into the ascending and descending branches. The ascending branch is expressed by the following rational function by Carreira-Chu [40],

$$x\le 1\quad y=\frac{nx}{n-1+x^n} \tag{7}$$

$$n=\frac{1}{1-\frac{f_c}{\varepsilon_0 E_c}} \tag{8}$$

where, $x=\varepsilon/\varepsilon_0$, $y=\sigma/f_c$, f_c is the axial compressive strength of the CA-UHPC at room temperature. According to the specification [41], the elastic modulus and peak strain are functions of the axial compressive strength,

$$E_c = 3959\sqrt{f_c} \tag{9}$$

$$\varepsilon_0 = 0.66(f_c)^{0.31} \tag{10}$$

The descending branch of the stress-strain curve of the CA-UHPC is expressed by the function proposed in GB 50010-2010 [29], with an additional parameter β. The expression is as follows,

$$x>1 \quad y = \frac{x}{\alpha(x-1)^{\beta} + x} \tag{11}$$

where, α and β are parameters related to the composition of the CA-UHPC.

The values of α and β at the room temperature, α_0 and β_0, can be data-fitted from the experiment on the CA-UHPC, as shown in Table 3. From section 3, the influence of coarse aggregate contents on the descending branch of the stress-strain curve should be taken into account. Therefore, based on the experimental results of this paper and in [42], different volume fraction of coarse aggregates (0~30%) and steel fibers (1%~2%) are considered in the descending branch equation. The calculation formula of α_0 and β_0 related to the volume fraction of coarse aggregates and steel fibers are proposed, as shown in Eq.(12) and Eq.(13),

$$\alpha_0 = \left(0.98 - 1.49V_{CA} + 4.74\left(V_{CA}\right)^2\right) \times (7.72 - 232.8V_{SF}) \tag{12}$$

$$\beta_0 = 0.79 \times \left(1.02 + 0.25V_{SF}\right) \tag{13}$$

where, V_{CA} refers to the volume fraction of coarse aggregates in the CA-UHPC; V_{SF} refers to the volume fraction of steel fibers in the CA-UHPC.

Table 3 Parameter values for the stress-strain curve model of the CA-UHPC at room temperature

Number	n	α_0	β_0	Eq.(12)	Eq.(13)	Calculated value/test value	
						α_0	β_0
CA0	13.31	2.970	0.995	3.003	0.81	1.011	0.814
CA10	15.33	2.742	1.222	2.690	0.81	0.981	0.663
CA20	16.75	2.594	0.979	2.666	0.81	1.028	0.827
CA30	21.5	2.947	0.981	2.929	0.81	0.994	0.825
					Average	1.003	0.782
					Coefficient of variation	0.0003	0.006

(2) High temperature parameters of the equation

From Eq.(1), Eq.(3), Eq.(5), Eq.(9) and Eq. (10), the elastic modulus $E_{cT}(T)$, peak strain $\varepsilon_{cT}(T)$, and axial compressive strength $f_{cT,U}$ under high temperature can be expressed as,

$$E_{cT}=\left(-\left(\frac{T-20}{1000}\right)+1\right)\times\left(3959\sqrt{f_c}\right) \tag{14}$$

$$\varepsilon_{cT}=\left(1.51\left(\frac{T-20}{1000}\right)+1\right)\times\left(0.66\left(f_c\right)^{0.31}\right) \tag{15}$$

$$f_{cT,U}=k_U\left(T\right)\times f_c \tag{16}$$

From the above equations and Eq.(8), the parameter n under high temperature, n_{UT}, of the ascending branch of the stress-strain curve under high temperature can be calculated. The values of α and β under high temperature, α_{UT} and β_{UT}, can be data-fitted from the experimental results of the stress-strain curves under high temperature. Thus,

$$\frac{\alpha_{UT}}{\alpha_0}=-74.02\left(\frac{T-20}{1000}\right)^3+76.46\left(\frac{T-20}{1000}\right)^2-6.44\left(\frac{T-20}{1000}\right)+1 \tag{17}$$

$$\frac{\beta_{UT}}{\beta_0}=5.94\left(\frac{T-20}{1000}\right)^3-9.56\left(\frac{T-20}{1000}\right)^2+5.1\left(\frac{T-20}{1000}\right)+1 \tag{18}$$

Using the formulas of n_{UT}, α_{UT} and β_{UT}, the calculated curves of the CA-UHPC under high temperature are plotted in Fig. 15 along with the respective experimental results. It can be seen that the predictions from the proposed equations agree well with the test results. It is noteworthy that the parameters of the predictive equations depend only on the temperature and the mix proportion of the CA-UHPC.

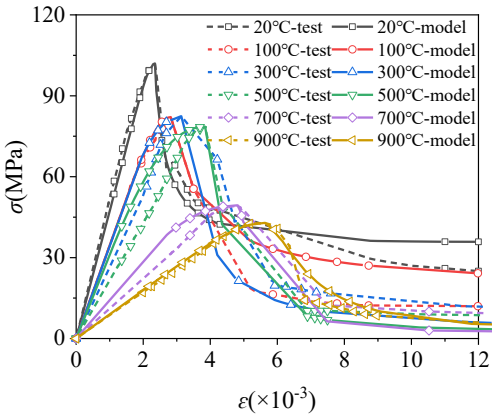

(a) CA0

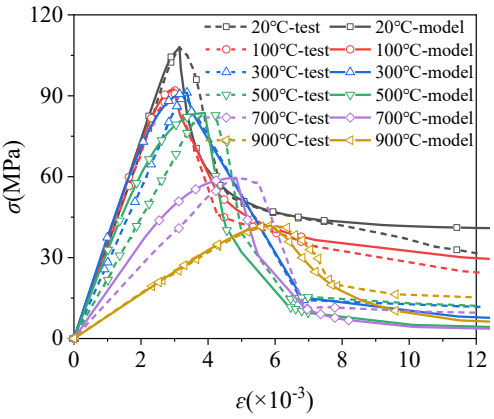

(b) CA10

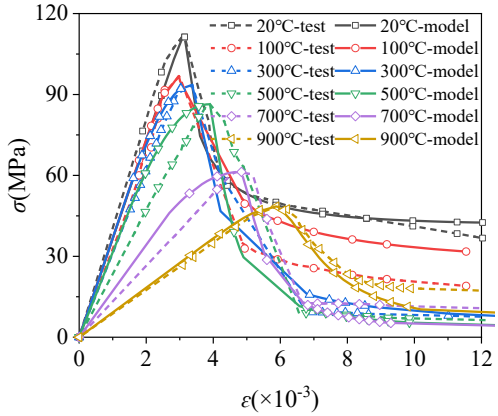

(c) CA20

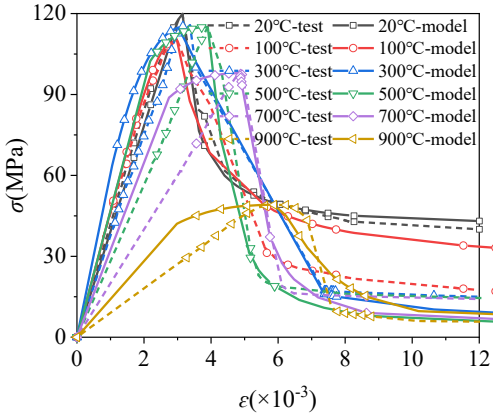

(d) CA30

Fig. 15 Stress-strain test curves and model curves under high temperature

5.2 Stress-strain equation after high temperature

From Eq.(2), Eq.(4), Eq.(6), Eq.(9) and Eq.(10), the elastic modulus $E_{cT}(T)$, peak strain $\varepsilon_{cT}(T)$, and $f_{cT,F}$ after high temperature can be expressed as,

$$E_{cT}=\left(-1.01\left(\frac{T-20}{1000}\right)+1\right)\times\left(3959\sqrt{f_c}\right) \tag{19}$$

$$\varepsilon_{cT}=\left(1.28\left(\frac{T-20}{1000}\right)^2-0.22\left(\frac{T-20}{1000}\right)+1\right)\times\left(0.66\left(f_c\right)^{0.31}\right) \tag{20}$$

$$f_{cT,F}=k_F\left(T\right)\times f_c \tag{21}$$

Using the above equations and Eq.(8), the parameter n after high temperature, n_{FT}, of the ascending branch of the stress-strain curve can be calculated. The values of α and β after high temperature, α_{FT} and β_{FT}, can be derived from data fitting of the experimental results.

$$\frac{\alpha_{FT}}{\alpha_0}=-6.77\left(\frac{T-20}{1000}\right)^3+7.55\left(\frac{T-20}{1000}\right)^2-0.88\left(\frac{T-20}{1000}\right)+1 \tag{22}$$

$$\frac{\beta_{FT}}{\beta_0}=6.55\left(\frac{T-20}{1000}\right)^3-7.64\left(\frac{T-20}{1000}\right)^2+2.43\left(\frac{T-20}{1000}\right)+1 \tag{23}$$

Using the parameter formulas of n_{FT}, α_{FT} and β_{FT}, Fig. 16 shows the comparson between the experimental and predicted stress-strain curves of the CA-UHPC after high temperature. It can be observed that the analytical formulas satisfactorily predict the stress-strain relation of the CA-UHPC after high temperature.

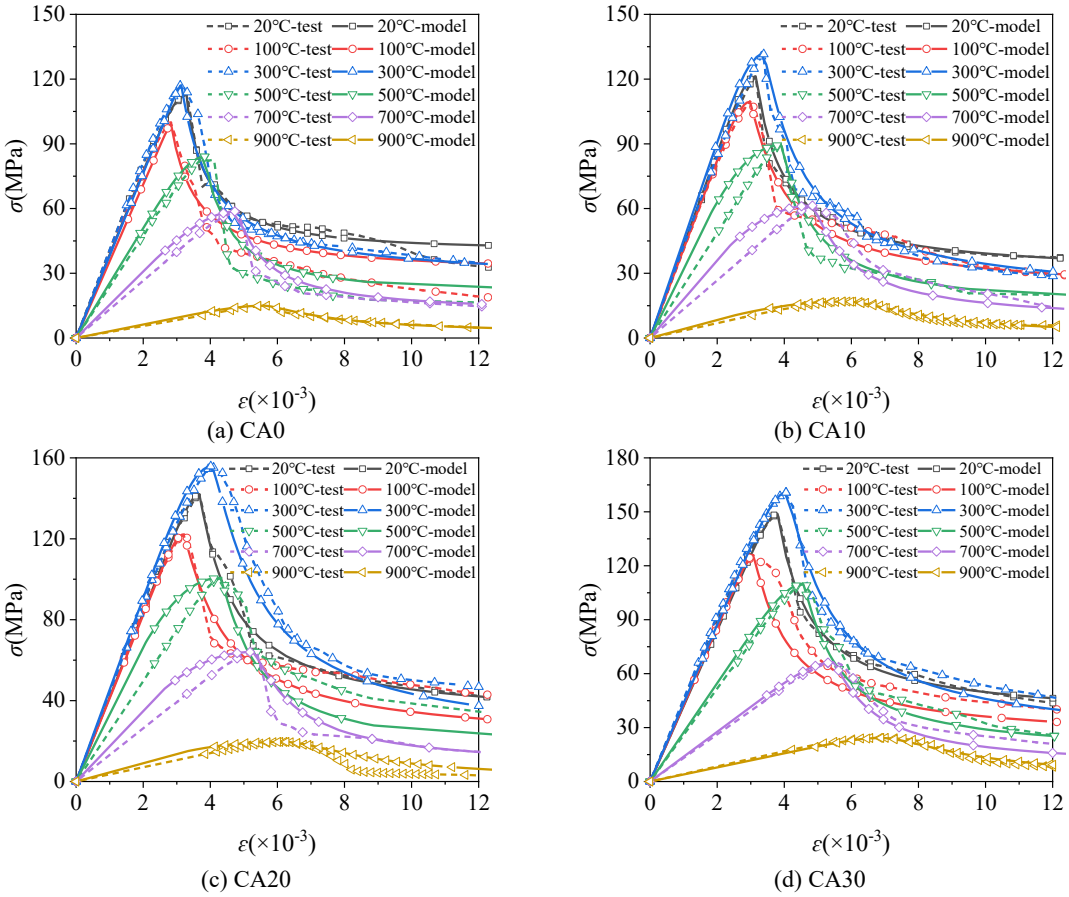

Fig. 16 Stress-strain test curves and model curves after high temperature

6 Conclusion

This paper systematically investigates the uniaxial compression of CA-UHPC under and after exposure to high temperatures. The main conclusions are as follows:

(1) The uniaxial compressive failure modes of the CA-UHPC under and after high temperatures are similar. All the specimens exhibit shear failure, with shear failure angles range from 60° to 85°. The angle between the main crack and the vertical direction increases with the increase of temperature. Except for the compression test under the temperature of 900°C, all the prisms maintain integrity after failure. Overall, the coarse aggregate contents have little effect on the failure mode.

(2) The axial compressive strength and elastic modulus under high temperature decreases almost linearly with the increase of temperature, while the axial compressive strength and elastic modulus after high temperature increases initially and then decreases. The peak strain under high temperature increases with the increase of temperature, while the peak strain after high temperature initially decreases and then increases. The elastic modulus and peak strain under and after high temperature increase with the increase of the coarse aggregate contents.

(3) Based on the experimental data, a procedure is proposed to determine the characteristic parameters of stress-strain curves under and after high temperatures, which are only temperature-dependent. Analytical equations of stress-strain curves for the CA-UHPC under and after high temperatures are also proposed and validated, relying solely on the temperature and mix proportion of the CA-UHPC.

Acknowledgement

The authors are grateful for the financial support from the National Natural Science Foundation of China (Grant No. 52178157, 51878518, 52278514) and scientific research fund support from Suzhou City University (Grant No. 3110709223, 5010701124).

References

[1] Ravichandran D, Prem P R, Kaliyavaradhan S K, et al. Influence of Fibers on Fresh and Hardened Properties of Ultra High Performance Concrete (UHPC)—a Review[J]. Journal of Building Engineering, 2022,57:104922.

[2] Yu J, Zhang B, Chen W, et al. Multi-Scale Analysis on the Tensile Properties of UHPC Considering Fiber Orientation[J]. Composite Structures, 2022,280:114835.

[3] Pan R, Song X, He W, et al. Direct Shear Strength of UHPC Considering Size Effect: Theoretical Model and Experimental Verification[J]. Journal of Building Engineering, 2023,71:106381.

[4] Bao J, Zheng R, Sun Y, et al. A State-of-the-Art Review on High Temperature Resistance of Lightweight Aggregate High-Strength Concrete[J]. Journal of Building Engineering, 2023,69:106267.

[5] Varona F B, Baeza F J, Bru D, et al. Influence of High Temperature on the Mechanical Properties of Hybrid Fibre Reinforced Normal and High Strength Concrete[J]. Construction and Building Materials, 2018,159:73-82.

[6] Mao Z, Zhang J, Li Y, et al. Performance Degradation and Microscopic Structure of Reactive Powder Concrete after Exposure to High Temperature [J]. Journal of Building Materials, 2022,25(12):1225-1232.

[7] Zheng W, Pan Z, Chen Z, et al. Shear Behavior of Reinforced Recycled Aggregate Concrete Beams after Exposure to Temperatures up to 600 °C[J]. Engineering Structures, 2021,244:112756.

[8] Peng G, Teng Y, Huang Y, et al. Fire Resistance of Ultra-high-performance Concrete with Coarse Aggregate: a Research Review [J]. Journal of North China Institute of Water Conservancy and Hydroelectric Power, 2013(01):1-6.

[9] Xue C, Yu M, Xu H, et al. Compressive Performance and Deterioration Mechanism of Ultra-High Performance Concrete with Coarse Aggregates under and after Heating[J]. Journal of Building Engineering, 2022:105502.

[10] Wang T, Yu M, Zhang X, et al. Post-Fire Mechanical Behaviour of Ultra-High-Performance Concrete-Filled Steel Tube (UHPCFST) Stub Columns Under Compression[J]. Journal of Constructional Steel Research, 2022,196:107384.

[11] Choe G, Kim G, Gucunski N, et al. Evaluation of the Mechanical Properties of 200 MPa Ultra-High-Strength Concrete at Elevated Temperatures and Residual Strength of Column[J]. Construction and Building Materials, 2015,86:159-168.

[12] Wang H, Lyu H, Liu T, et al. Effect of Post-Fire Curing on Compressive Strength of Ultra-High Performance Concrete and Mortar[J]. Construction and Building Materials, 2022,346:128447.

[13] Suescum-Morales D, Ríos J D, De La Concha A M, et al. Effect of Moderate Temperatures on Compressive Strength of Ultra-High-Performance Concrete: a Microstructural Analysis[J]. Cement and Concrete Research, 2021,140:106303.

[14] Zhu Y, Hussein H, Kumar A, et al. A Review: Material and Structural Properties of UHPC at Elevated Temperatures or Fire Conditions[J]. Cement and Concrete Composites, 2021,123:104212.

[15] Tang J, Ma W, Pang Y, et al. Uniaxial Compression Performance and Stress-Strain Constitutive Model of the Aluminate Cement-Based UHPC after High Temperature[J]. Construction and Building Materials, 2021,309:125173.

[16] Tai Y, Pan H, Kung Y. Mechanical Properties of Steel Fiber Reinforced Reactive Powder Concrete Following Exposure to High Temperature Reaching 800°C[J]. Nuclear Engineering and Design, 2011,241(7):2416-2424.

[17] Zheng W, Li H, Wang Y. Compressive Stress-Strain Relationship of Steel Fiber-Reinforced Reactive Powder Concrete after Exposure to Elevated Temperatures[J]. Construction and Building Materials, 2012,35:931-940.

[18] Zheng W, Li H, Wang Y. Compressive Stress-Strain Relationship of Hybrid Fiber-Reinforced Reactive Powder Concrete after Exposure to High Temperature [J]. Journal of Building Materials, 2013,16(03):388-395.
[19] Fan J. Experimental Study on Compression Performance of Calcium Aluminate Cement Based Ultra High Performance Concrete Exposed to Elevated Temperatures [D]. Zhengzhou: Zhengzhou University, 2021.
[20] Xu F. Experimental Research on Fire Performance of Steel Fiber Reactive Powder Concrete [D]. Harbin: Harbin Institute of Technology, 2011.
[21] Zheng W, Luo B, Wang Y. Compressive and Tensile Properties of Reactive Powder Concrete with Steel Fibres at Elevated Temperatures[J]. Construction and Building Materials, 2013,41:844-851.
[22] Zheng W, Luo B, Wang Y. Stress-Strain Relationship of Steel-Fibre Reinforced Reactive Powder Concrete at Elevated Temperatures[J]. Materials and Structures, 2015,48(7):2299-2314.
[23] Huang L, Du Y, Zhu S, et al. Material Property and Constitutive Model of C120 Hybrid Fiber Ultra-High Performance Concrete at Elevated Temperatures[J]. Structures (Oxford), 2023,50:373-386.
[24] Xue C, Yu M, Xu H, et al. Experimental Study on Thermal Performance of Ultra-High Performance Concrete with Coarse Aggregates at High Temperature[J]. Construction and Building Materials, 2022,314:125585.
[25] Kodur V, Banerji S, Solhmirzaei R. Effect of Temperature on Thermal Properties of Ultrahigh-Performance Concrete[J]. Journal of Materials in Civil Engineering, 2020,32(8).
[26] Eurocode 2: Design of Concrete Structures-Part 1-2: General Rules-Structural Fire Design[S]. Brussels: CEN: 2004.
[27] Guo Z, Shi X. High Temperature Performance and Calculation of Reinforced Concrete [M]. Beijing: Tsinghua University Press, 2003.
[28] Yu M, Xue C, Xu H, et al. An auxiliary Device for Axial Compression Test of Quasi Brittle Materials under High Temperatures: 2022.06.07.
[29] GB 50010-2010 Code for Design of Concrete Structures [S]. Beijing: China Construction Industry Press, 2010.
[30] Zhao H, Wang Y, Liu F. Stress-Strain Relationship of Coarse RCA Concrete Exposed to Elevated Temperatures[J]. Magazine of Concrete Research, 2017,69(13-14):649-664.
[31] Terro M J. Numerical Modeling of the Behavior of Concrete Structures in Fire[J]. 1998.
[32] Guo Z. High Strength and Deformation of Concrete - Experimental Basis and Constitutive Relationship [M]. Beijing: Tsinghua University Press, 2003.
[33] Xiong M, Liew J Y R. Mechanical Behaviour of Ultra-High Strength Concrete at Elevated Temperatures and Fire Resistance of Ultra-High Strength Concrete Filled Steel Tubes[J]. Materials & Design, 2016,104:414-427.
[34] Luo B. Study on Explosive Spalling Rules and Mechanical Properties of Reactive Powder Concrete at Elevated Temperatures [D]. Harbin: Harbin Institute of Technology, 2014.
[35] Banerji S, Kodur V. Effect of Temperature on Mechanical Properties of Ultra-High Performance Concrete[J]. Fire and Materials, 2021.
[36] BS EN 1994-1-2:2005 Eurocode 4-Design of Composite Steel and Concrete Structures -Part 1-2: General Rules - Structural Fire Design[S]. 1994.
[37] Wu B, Ma Z, Ou J. Experimental Research on Deformation and Constitutive Relationship of Concrete under Axial Loading and High Temperature [J]. Journal of Building Structures, 1999(05):42-49.
[38] Chang Y, Chen Y, Sheu M, et al. Residual Stress-Strain Relationship for Concrete after Exposure to High Temperatures[J]. Cement and Concrete Research, 2006,36(10):1999-2005.
[39] Aslani F, Samali B. Constitutive Relationships for Self-Compacting Concrete at Elevated Temperatures[J]. Materials and Structures, 2015,48(1-2):337-356.
[40] Carreira D J, Chu K. Stress-Strain Relationship for Plain Concrete in Compression[J]. ACI, 1986.
[41] Fib Model Code for Concrete Structures 2010[S]. Lausanne, Switzerland: International Federation for

Structural Concrete, 2013.
[42] Wang S. Research on the Elastoplastic Damage Constitutive Relationship of Ultra-High Performance Concrete [D]. Wuhan: Wuhan University, 2022.